IDETC2019-98291

REDUCED-ORDER MODELING AND EXPERIMENTAL STUDIES OF TWO-WAY COUPLED FLUID-STRUCTURE INTERACTION IN FLAPPING WINGS

Ryan K. Schwab* Graduate Researcher rschwab03@gmail.com Heidi E. Reid* Graduate Researcher heidi.reid@montana.edu Mark A. Jankauski Assistant Professor mark.jankauski@montana.edu

Montana State University
Department of Mechanical & Industrial Engineering
Bozeman, MT 59717

ABSTRACT

Flapping, flexible wings deform under both aerodynamic and inertial loads. However, the fluid-structure interaction (FSI) governing flapping wing dynamics is not well understood. Conventional FSI models require excessive computational resources and are not conducive to parameter studies that consider variable wing kinematics or geometry. Here, we present a simple twoway coupled FSI model for a wing subjected to single-degree-offreedom (SDOF) rotation. The model is reduced-order and can be solved several orders of magnitude faster than direct computational methods. We construct a SDOF rotation stage and measure basal strain of a flapping wing in-air and in-vacuum to study our model experimentally. Overall, agreement between theory and experiment is excellent. In-vacuum, the wing has a large 3ω response when flapping at approximately 1/3 its natural frequency. This response is attenuated substantially when flapping in-air as a result of aerodynamic damping. These results highlight the importance of two-way coupling between the fluid and structure, since one-way coupled approaches cannot describe such phenomena. Moving forward, our model enables advanced studies of biological flight and facilitates bio-inspired design of flapping wing technologies.

NOMENCLATURE

FWMAV Flapping wing micro air vehicle
FSI Fluid-structure interaction
CFD Computational fluid dynamics
FEA Finite element analysis
SDOF Single degree-of-freedom
MDOF Multiple degree-of-freedom
BET Blade element theory

INTRODUCTION

EoM Equation of motion

Flapping, flexible wings are integral elements in several emerging technologies, such as flapping wing micro air vehicles (FW-MAVs) as well as elastic airfoil energy harvesting devices. FW-MAVs are a robotic platform [1–3] that could enable low-cost remote sensing with unprecedented spatial resolution. Foil-based energy harvesters have the potential for highly efficient energy extraction from ambient flows [4–6] and could power the extensive sensor networks employed in many "Internet of Things" applications. But while such technologies could expedite the realization of smart national infrastructure, they remain in their infancy stages. This is primarily because the physics governing flapping wings is not well understood.

As a wing flaps, it deforms under both fluid and structural loads. This fluid-structure interaction (FSI) plays a critical role in

^{*}Authors contributed equally to this publication.

flapping wing dynamics. Despite the significance of FSI to flapping wing flight, we know relatively little about it. Conventional models of flapping wing FSI require long solution times and are consequently ill-suited for broad parametric studies considering variables such as flapping kinematics, frequency and wing geometry. The ability to carry out parametric studies fast and efficiently is critical to design of flapping wing based technologies.

High-order FSI models often rely on direct computational methods, such as finite element analysis (FEA) and computational fluid dynamics (CFD) [7–11]. Each of these computational methods face considerable inefficiencies in calculating flapping wing dynamics. CFD must resolve the flow field over an entire control volume in order to estimate the pressure distribution over the wing surface [12]. This often requires solving several thousands of equations which makes CFD computationally intensive. Moreover, large flapping rotations lead to periodic centrifugal forces that cause FEA stiffness matrices to become timevarying [13]. If direct FEA is used to calculate wing deformation, the stiffness matrix must be updated at each interval of analysis. The result is a huge number of degrees of freedom (DOF), and the time required to evaluate the response of all DOF is extensive. Then, when FEA and CFD are coupled together to solve a full FSI problem, the inefficiencies of each solver are compounded and solution times become intractable.

In an effort to reduce computational complexity, many researchers leverage quasi-static methods rooted in blade element theory (BET) [14–17]. BET discretizes a wing into airfoils (blade elements) that run along the wing's chord. The elemental aerodynamic forces are estimated over each individual blade using 2D airfoil theory and are then integrated over the wing to calculate net aerodynamic forces. While this is an efficient method to estimate aerodynamics, BET is generally limited to rigid wings. It has been used only a handful of times to address the effects of wing flexibility.

Wang et al. developed a flapping wing FSI model based upon BET, however the wing's leading edge was assumed rigid and consequently the model could only estimate torsional deformation and not bending deformation [18]. Stanford et al. developed a FSI model that can account for bending, but their structural solver requires each *physical* DOF be solved for [19]. They did not leverage modal truncation to reduce the order of the structural model. Jankauski developed a reduced-order aeroelastic framework for flapping wings using modal truncation and BET, however this framework was used only to study one-way coupled FSI where the fluid was able to affect the structure but not visa versa [20]. It is possible that two-way coupling between fluid and structure is important to flapping wing dynamics. Moreover, each of these three studies are computational in nature; none of the aforementioned models were verified experimentally.

Given the motivation, the objective of this research is to develop a reduced-order two-way coupled FSI model of a flapping wing and to study this model through a simple experiment.

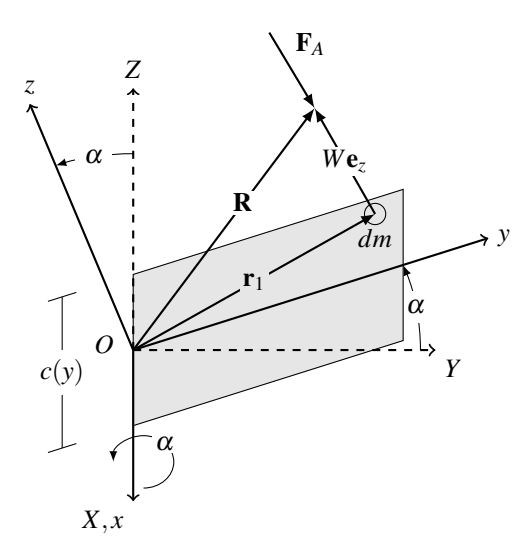


FIGURE 1: WING DRAWN IN ROTATING REFERENCE FRAME. POSITION VECTOR \mathbf{R} DRAWN FROM FIXED POINT OF ROTATION O TO AN ARBITRARY DIFFERENTIAL MASS ELEMENT. \mathbf{F}_A IS THE AERODYNAMIC FORCE ACTING NORMAL TO THE WING SURFACE.

Due to the complexity of two-way coupled FSI, we will initially restrict our model to single-degree-of-freedom (SDOF) rotation. Moving forward, we will generalize this to more realistic multiple-degree-of-freedom (MDOF) flapping. The remainder of the paper is organized as follows. First, we derive the FSI model using the Lagrangian approach for the structural equation of motion (EoM) and BET for the fluid model. Next, we detail a simple SDOF flapping experiment used to study our model. We then compare simulation results to experimental findings and discuss the implications of aerodynamics on the wing's structural response. We conclude by making brief remarks on how our findings inform biological flight as well as the design of flapping wing technologies.

THEORY

Here, we derive a reduced-order two-way coupled FSI model for flexible wings subject to SDOF flapping. We begin by determining the structural EoM via the Lagrangian method. We then identify aerodynamic forces and coupling through a BET approach. Aerodynamic terms are included in the EoM using the principle of virtual work.

Structural Model

The aeroelastic model in this section originated in [13, 20] for a wing rotating in three dimensions; here, we consider only SDOF rotation. The model is summarized briefly only to provide clarity

to this manuscript. For a more thorough treatment, the reader is directed to these references.

We assume an inertial X - Y - Z coordinate frame undergoes a finite rotation about X with rotation amplitude α . The resulting x - y - z coordinate frame is bound to the rigid body rotation of the wing (Fig. 1) and has an angular velocity

$$\mathbf{\Omega} = \dot{\alpha} \, \mathbf{e}_{x} \tag{1}$$

In the rotating coordinate frame, we draw a position vector \mathbf{R} from the reference frame origin O to an arbitrary differential mass dm. Position vector \mathbf{R} is

$$\mathbf{R} = \mathbf{r}_1 + W(\mathbf{r}_1, t)\mathbf{e}_z \tag{2}$$

where \mathbf{r}_1 describes the planar coordinates of dm with respect to the x-y-z frame (e.g., $\mathbf{r}_1=x\mathbf{e}_x+y\mathbf{e}_y$) and $W(\mathbf{r}_1,t)$ is an infinitesimal out-of-plane deflection dependent on both space and time. In-plane deformation is neglected. The velocity of dm is

$$\dot{\mathbf{R}} = \mathbf{\Omega} \times \mathbf{R} + \dot{W} \mathbf{e}_{\tau} \tag{3}$$

Note that \mathbf{e}_z is constant with respect to the x-y-z terminal frame and therefore has a time derivative of zero. Then, deflection $W(\mathbf{r}_1,t)$ is expanded as

$$W(\mathbf{r}_1,t) = \sum_{k=1}^{\infty} \phi_k(\mathbf{r}_1) q_k(t)$$
 (4)

where ϕ_k is the k^{th} mode shape and q_k is the k^{th} modal response to be determined. We normalize ϕ_k with respect to the wing mass such that it satisfies orthonormal conditions. Finally, we determine the total kinetic and potential energies of the wing and use the Lagrangian approach to determine the EoM governing modal response q_k as

$$\ddot{q}_k + 2\zeta_k \omega_k \dot{q}_k + (\omega_k^2 - \dot{\alpha}^2) q_k = \ddot{\alpha} \int_m y \, \phi_k \, dm + Q_k \qquad (5)$$

where ω_k is the wing's k^{th} natural frequency, ζ_k is the damping ratio of the k^{th} mode and Q_k are non-conservative modal forces from aerodynamic loading. The explicit form of Q_k is detailed in the following section. Note that the modal damping term above does not explicitly appear in the derivation but is added as a correction factor after the undamped EoM is formulated.

Once modal responses q_k are known, physical quantities

such as wing strain can easily be estimated. In this work, we measure wing strain rather than deformation to assess model accuracy. Physical strain is determined at \mathbf{r}_1 by

$$\varepsilon(\mathbf{r}_1,t) = \sum_{k=1}^{\infty} \varepsilon_k q_k \tag{6}$$

where ε_k is modal strain.

Aerodynamic Modeling and Fluid-Structure Coupling

Now, we determine the aerodynamic modal force Q_k . We use a simple quasi-steady formulation and assume that unsteady fluid phenomena are negligible. We assume an aerodynamic force per unit area \mathbf{F}_A acting normal to a differential surface on the wing is

$$\mathbf{F}_{A} = -\frac{1}{2}C\rho_{f}\,\dot{\mathbf{R}}\cdot\dot{\mathbf{R}}\,\mathrm{sgn}(\dot{\mathbf{R}})\,\mathbf{e}_{z} \tag{7}$$

where ρ_f is the density of air and C is a general aerodynamic coefficient. The $\operatorname{sgn}(\mathbf{R})$ ensures that the aerodynamic force is acting in the direction opposite to the instantaneous velocity along at any point on the surface. For the purposes of this work, we assume the aerodynamic force does not vary along the wing chord. This implies that the aerodynamic force does not vary with respect to the x component of \mathbf{r}_1 (Fig. 1). While this simplification is suitable for the simple wing geometry and SDOF kinematics considered in this work, it must be relaxed for more complex wing geometries or flapping kinematics.

Moreover, because we assume SDOF rotation, we consider only aerodynamic drag in this work. Aerodynamic lift or rotational forces associated with dynamic pitching do not affect wing deformation during SDOF rotation. However, the above form is general and could be used to include lift or other aerodynamic forces as well should one consider more complex kinematics. The primary difference between force types will be the selection of empirical coefficient *C*.

Then, expanding the above expression of \mathbf{F}_A and neglecting terms of $\mathcal{O}(W^2)$ or higher, we find

$$\mathbf{F}_{A} = -\frac{1}{2}C\rho_{f}\left(2\dot{\alpha}\dot{W}y + \dot{\alpha}^{2}y^{2}\right)\operatorname{sgn}(\dot{\mathbf{R}})\mathbf{e}_{z} \tag{8}$$

where y is the y-axis component of \mathbf{r}_1 (Fig. 1) where \mathbf{F}_A is assumed to act. Substituting the eigenfunction expansion of out-of-plane elastic deformation W gives

$$\mathbf{F}_{A} = -\frac{1}{2}C\rho_{f} \left[\sum_{k=1}^{\infty} \left(2\dot{\alpha}\dot{q}_{k}\phi_{k}y \right) + \dot{\alpha}^{2}y^{2} \right] \operatorname{sgn}(\dot{\mathbf{R}}) \mathbf{e}_{z}$$
 (9)

Next, we project the physical aerodynamic force into the modal domain using the principle of virtual work. The virtual work δW done by \mathbf{F}_A is

$$\delta \mathcal{W} = \int_{S} \mathbf{F}_{A} \cdot \delta W \, \mathbf{e}_{z} \, dS \tag{10}$$

$$\delta \mathcal{W} = \int_{S} \mathbf{F}_{A} \cdot \sum_{k=1}^{\infty} \phi_{k} \delta q_{k} \, \mathbf{e}_{z} \, dS \tag{11}$$

where dS is the differential surface over which the aerodynamic force acts. Recognizing that dS is simply wing chord width c(y) multiplied by differential length dy, we expand the above to

$$\delta \mathcal{W} = -\frac{1}{2}C\rho_f \left[\int_{y} \left(\sum_{r=1}^{\infty} (2\dot{\alpha}\dot{q}_r \phi_r y) + \dot{\alpha}^2 y^2 \right) c(y) \, dy \right] \dots \\ \dots * \sum_{k=1}^{\infty} \phi_k \delta q_k \operatorname{sgn}(\dot{\mathbf{R}})$$
(12)

where * indicates scalar multiplication. Note that we have included a second modal index r which also contains the k^{th} mode shape. Then, the non-conservative aerodynamic modal force corresponding to the k^{th} vibration mode, denoted Q_k , is

$$Q_{k} = \underbrace{-\frac{1}{2}C\rho_{f}[\dot{\alpha}^{2}\int_{y}y^{2}c(y)\phi_{k}dy}_{Q_{A,k}}... + 2\dot{\alpha}\sum_{r=1}^{\infty}\int_{y}\dot{q}_{r}\phi_{r}\phi_{k}yc(y)dy]\operatorname{sgn}(\dot{\mathbf{R}})}_{Q_{C,k}}$$
(13)

The first term of Q_k is simply an independent aerodynamic modal force term dependent only on time. We denote this term $Q_{A,k}$ for later reference. The second term, labeled $Q_{\zeta,k}$, is more complex. Generally speaking, it appears as an aerodynamic damping term that may collectively dissipate energy from all wing vibration modes. This term effectively couples these modes together. Depending on the sign of \dot{q}_k and $\mathrm{sgn}(\dot{\mathbf{R}})$, it may appear as a negative damping term as well. If so, energy may be added to the wing which will eventually cause it to go unstable.

EXPERIMENT

In this section, we describe a simple experiment designed to study the FSI model. We construct a SDOF rotation stage to prescribe flapping kinematics to a rectangular paper wing. Mode shapes and natural frequencies of the paper wing are estimated via FEA and are subsequently verified using a scanning vibrometer. During flapping experiments, we measure the spanwise strain at a point near the base of the wing using a uniaxial strain gage. We conduct flapping experiments both in-vacuum and in-air. Details are as follows.

Rotation Stage

The SDOF rotation stage is pictured in Figure 2. All mounting brackets are 3D printed with FormLabs durable resin. A 60 W DC motor (Maxon Motors, 310007) drives the motion of the wing. The motor is equipped with an optical encoder that provides position feedback to a motor controller/driver (Maxon Motors, EPOS 24/5). The motor controller uses a PID framework to maintain prescribed flapping kinematics and minimize overshoot. All motion profiles are prescribed through a laptop computer running Labview. In this work, we consider discrete flapping frequencies ranging from 5 - 15 Hz and a rotation amplitude of 45°. All rotations are sinusoidal. Each trial at a particular flapping frequency is conducted three times and the measurements from each trial are averaged in the frequency domain.

The motor connects to a wing clamp through a shaft coupler. The clamp secures the wing edge. A 350 ohm strain gage (Omega Engineering, GD-2/350-DY11) is adhered near the wing base. We use a National Instruments NI 9236 cDAQ module to provide excitation voltage to the gage as well as to record the temporal strain during experiments. The wing clamp is terminated with a low friction flange mount ball bearing. A female-end quantized analog encoder (US Digital, MAE3-A10-250-220-7-B) records the angular position of the terminated shaft end.

The entire rotation stage is housed in an acrylic vacuum chamber (Sanatron, Fig. 3) capable of operating at pressures as low as 500 milliTorr. At this pressure, the medium density is

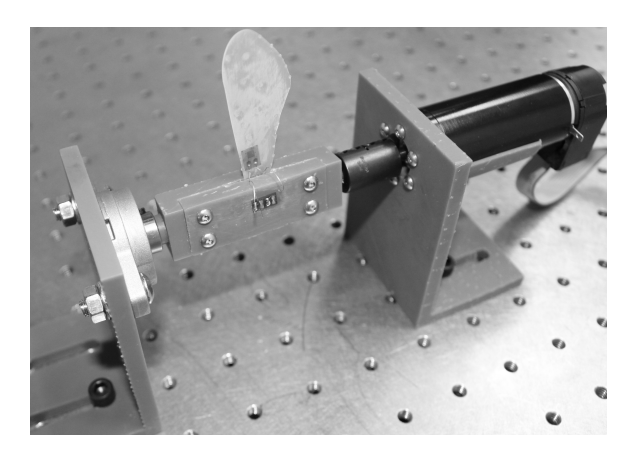


FIGURE 2: DC MOTOR DRIVEN SDOF ROTATION STAGE USED FOR FSI EXPERIMENTS. PLEASE NOTE THE WING SHOWN ABOVE DIFFERS FROM THE PAPER WING USED IN THE EXPERIMENT.



FIGURE 3: ACRYLIC VACUUM CHAMBER CONSTRUCTED BY SANATRON.

roughly 0.05% of ambient air. All vacuum feed-through components are provided by Kurt J. Lesker company. The ability to conduct experiments in-vacuum allows us to evaluate the accuracy of the structural model prior to investigating the FSI model.

Experimental Paper Wing

We use a simple rectangular paper wing in all flapping experiments. The wing is made of thick card stock and is cut with a shear. We design this wing to be (1) roughly the same length and aspect ratio of a hawkmoth M. sexta wing and (2) to have a natural frequency less than 45 Hz. The wing is designed to have a natural frequency less than this value because we wish to observe a 3ω resonance response and our rotation stage has a maximum flapping rate around 15 Hz. The wing is weighed using a scale and measured using a digital caliper. Young's moduli are taken from available literature values. All material and geometric properties of the wing and the strain gage mounted to the wing are shown in Table 1.

We model the experimental wing in ABAQUS FEA to determine its natural frequencies and mode shapes. The FEA model

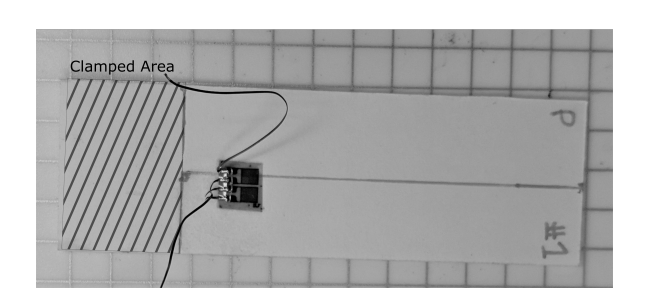


FIGURE 4: EXPERIMENTAL PAPER WING ON GRIDDED MAT. EACH GRID BOX IS 5 MM ×5 MM. CROSS HATCHED AREA INDICATES CLAMPED BOUNDARY CONDITION.

TABLE 1: EXPERIMENTAL WING PROPERTIES.

Variable	Description	Value	Unit
L_w	Wing Unclamped Length	5	cm
W_w	Wing Width	2	cm
t_w	Wing Thickness	0.17	mm
E_w	Wing Young's Modulus	9.5	GPa
L_g	Gage Length	5.65	mm
W_g	Gage Width	6.35	mm
t_g	Gage Thickness	0.13	mm
E_g	Gage Young's Modulus	2.5	GPa
m	Total Mass	0.21	grams

assumes the wing is clamped at its base edge (Fig. 4) which implies no rotation or translation in this clamped region. We include the strain gage in the FEA model because it has a thickness on the same order of magnitude as the paper. According to the manufacturer, the gage is composed primarily of polyimide film. As a result, the gage locally stiffens the wing in a way that cannot be neglected. For this work, we retain only a single vibration mode. Across the experimental parameters considered, higher-order modes had a negligible contribution to the wing's dynamic response. The first natural frequency predicted via FEA is ω_1 = 31.5 Hz and corresponds to a bending mode (Fig. 6).

Next, we verify FEA-predicted mode shapes and natural frequencies experimentally. Because the wing is lightweight and has a large surface area, we measure these parameters in-air as well as in-vacuum to remove added mass effects. We secure the paper wing to a modal shaker (Modal Shop, K2007E007) using a metal clamp. The shaker excites the wing at its base via a linear swept sine signal ranging from 10 - 1000 Hz over 3.2 seconds. We measure basal excitation with a piezoelectric accelerometer (PCB Piezotronics, 352A21) and the response velocity of the wing at several points using a planar scanning vibrometer (Polytec PSV-400). We acquire data at 2.56 kHz, which results in a spectral resolution of 3200 FFT lines over the frequency range considered. We average the frequency response function over three trials at each measurement point to reduce spectral noise. Measured responses are reconstructed to identify the first vibration mode shape. This mode shape agrees well with that determined via FEA (Fig. 6). We then calculate the frequency response function averaged over the wing surface $G(\omega)$ and use FEMTools modal parameter extractor to estimate the first natural frequency and damping ratio from this averaged frequency response (Tab. 2).

Overall, the agreement between natural frequencies calculated via FEA ($\omega_1 = 31.5 \text{ Hz}$) and measured experimentally (ω_1 = 30.2 Hz) is good. We consider the natural frequency measured in-vacuum for this comparison. The discrepancy is likely because the boundary conditions in simulation and experiment are slightly disparate. Even for the simple boundary condition shown in Fig. 4, it is challenging to experimentally clamp the wing at the precise location used in FEA. Even minor changes in wing's free length will affect its natural frequency. The natural frequency in-air is slightly lower than that measured in-vacuum due to added mass. We also observe that the damping ratio is greater in-air, which suggests that aerodynamic damping may affect the structural response during flapping experiments. We found no notable differences between the mode shape measured in-air and in-vacuum. For the simulations that follow, we use experimentally measured natural frequencies and damping ratios rather than those determined via FEA.

TABLE 2: EXPERIMENTALLY MEASURED NATURAL FREQUENCY AND DAMPING RATIO FOR FIRST VIBRATION MODE OF PAPER WING IN-AIR AND IN-VACUUM.

	Air	Vacuum
Natural Frequency ω_1	29.06 Hz	30.23 Hz
Damping Ratio ζ_1	1.29 %	0.89 %

Wing Frequency Response Function Magnitude

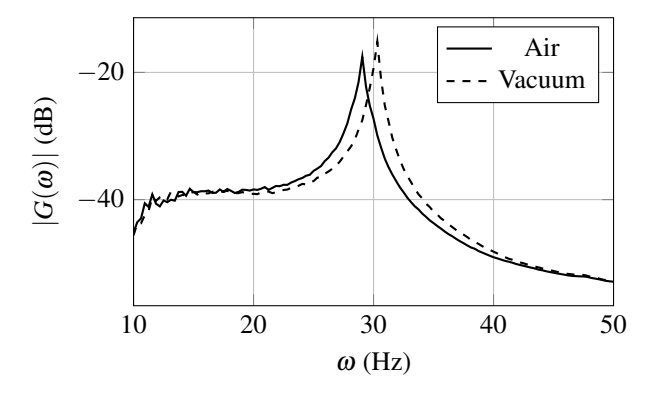


FIGURE 5: MAGNITUDE OF WING FREQUENCY RESPONSE FUNCTION RELATING BASE ACCELERATION TO AVERAGED OUTPUT VELOCITY.

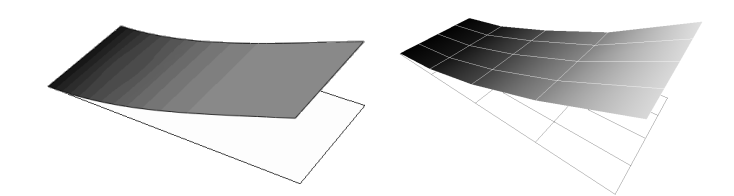


FIGURE 6: FIRST VIBRATION MODE SHAPE OF PAPER WING. (LEFT) PREDICTED VIA FEA, (RIGHT) MEASURED EXPERIMENTALLY.

RESULTS

We begin this section by comparing structural model predictions to measurements taken from a wing flapping in-vacuum. We next compare FSI model predictions to measurements taken from a wing flapping in-air. We conclude by investigating the FSI model to provide insight to aerodynamic damping mechanisms observed during the experiments.

Model-Theory Comparison

We first evaluate our structural model (Eq. 5) when Q_k =0. We compare predictions made by this model to strain of a wing flapping in-vacuum. Eq. 5 is solved numerically over 50 periods for each flapping frequency to find the modal response. Then, strain at the strain gage location is determined through Eq. 6. We take the Fourier transform to identify peak-to-peak strain at the driving frequency and each harmonic thereof. Across the range of flap frequencies ω considered, we only observe considerable response components at ω and 3ω . We show the magnitude of these components as a function of flapping frequency ω in Fig. 7.

In general, agreement between the structural model and the experimental results is fairly good, particularly at the primary response magnitude. The largest discrepancy occurs at the third harmonic of strain. It appears the experimental 3ω strain maxima occurs between 30 - 31.5 Hz, slightly higher than is predicted by the model. We also note that the experimental strain peak at 3ω is less abrupt than the model indicates. It is possible the wing is having large enough deflections that nonlinear damping becomes nontrivial. This would increase response magnitude at frequencies immediately surrounding the strain peak. For large oscillations, the damping ratio in some structures increases monotonically with respect to oscillation amplitude [21].

One result we would like to point out is the significant 3ω response when $\omega=10$ Hz. The peak-to-peak strain magnitude is almost identical at the flap frequency and the third harmonic of the flap frequency here. This is surprising given that the excitation term in Eq. 5 has only an ω component. However, due to the time-varying stiffness in the EoM, excitation terms at ω will generate odd harmonics in the modal response [22]. Since the natural frequency of the wing is roughly 30 Hz, a 10 Hz flapping

frequency is expected to cause a near-resonance of the wing. It is interesting to see whether aerodynamics will amplify or damp this response.

Now that we have verified that the structural model accurately predicts in-vacuum dynamics, we repeat the flapping experiment in-air. We include the aerodynamic modal forces given by Eq. 13 into the EoM. We assume the aerodynamic drag coefficient is C=3.0 and the density of air is $\rho_f=1.22$ kg/m³. The comparison between FSI model predictions and experimental results is shown in Figure. 8.

The model-theory agreement is excellent. There are no notable discrepancies to address. Interestingly, the 3ω strain response that was apparent in-vacuum is substantially reduced inair. This is a direct result of aerodynamic damping, which is discussed in greater detail in the following subsection. We no longer observe any evidence of nonlinear structural damping. This is perhaps because the wing tip deflections immediately around this flapping frequency are smaller than those seen in-vacuum.

As important, the model solves extremely efficiently; on a standard laptop, we are able to predict the response over a flapping cycle in a mere 0.075 seconds. This time can further be reduced by optimizing simulation parameters or by using faster processors. Unfortunately, we were unable to find any reported

Strain Magnitude vs. Flap Frequency, In-Vacuum

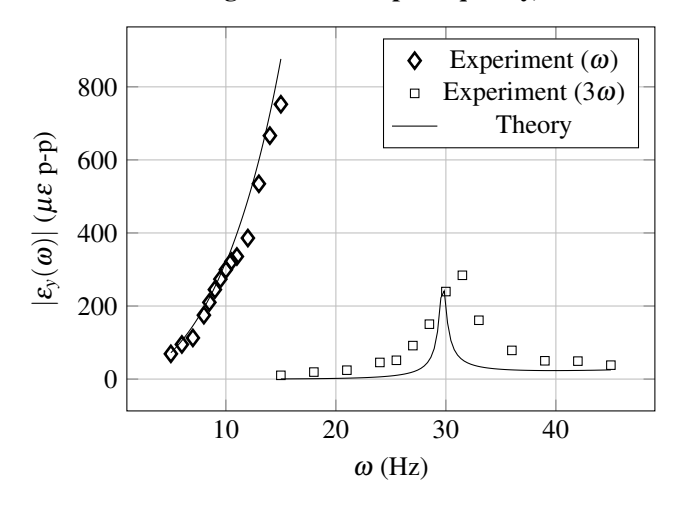


FIGURE 7: STRAIN MAGNITUDE AS A FUNCTION OF FLAPPING FREQUENCY FOR IN-VACUUM FLAPPING EXPERIMENTS. EQUATION 5 IS USED TO MAKE THEORETIC PREDICTIONS WITH Q_K =0. EACH DIAMOND REPRESENTS THE AVERAGE OF THREE 20-SECOND FLAPPING TRIALS AT A PARTICULAR FLAPPING FREQUENCY. NOTE THAT FLAPPING FREQUENCIES RANGE FROM 5 - 15 HZ AND 3 ω HARMONICS OF THE FLAPPING FREQUENCY RANGE FROM 15 - 30 HZ.

computation times of direct FSI methods for comparison. However, in the past we have used CFD to calculate pressure distributions over a rigid flapping wing. Using a relatively coarse time step and surface mesh, it required approximately one hour per wingbeat to resolve to the flow field – and this is without considering fluid-structure coupling. Thus, we estimate our new model predicts the wing response *at least* 4 orders of magnitude faster than direct FSI methods. In reality, the computational savings are likely even greater.

Aerodynamic Damping

In the previous section, we observed a large 3ω dynamic response when the wing's flapping frequency was roughly 1/3 of its first natural frequency. The 3ω response was especially pronounced for the wing flapping in-vacuum but was reduced significantly in-air. Here, we aim to identify the aerodynamic mechanism responsible for attenuating the 3ω response.

According to our model, there are two ways that aerodynamics can reduce the 3ω wing response. The first is through the time-dependent aerodynamic modal force $Q_{A,k}$. If we consider only $Q_{A,k}$ and neglect the aerodynamic damping term $Q_{\zeta,k}$, we ultimately have a one-coupled FSI model because $Q_{A,k}$ depends only on time and not wing deformation. On the other hand, by including $Q_{\zeta,k}$, we allow coupling between structural defor-

Strain Magnitude vs. Flap Frequency, In-Air

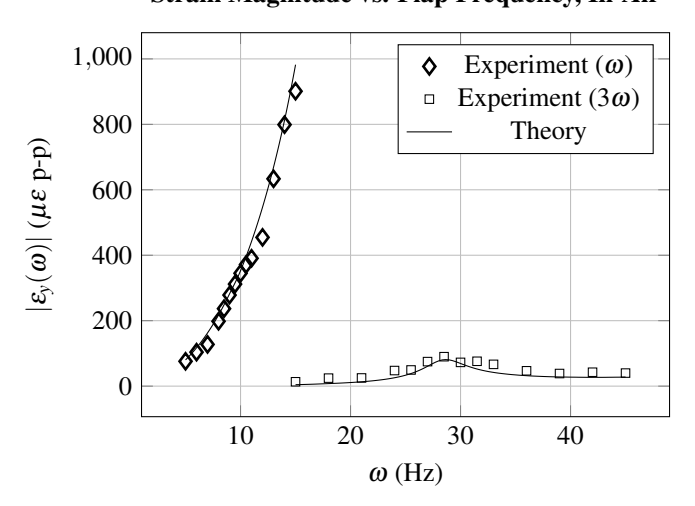


FIGURE 8: STRAIN MAGNITUDE AS A FUNCTION OF FLAPPING FREQUENCY FOR IN-AIR FLAPPING EXPERIMENTS. EACH DIAMOND REPRESENTS THE AVERAGE OF THREE 20-SECOND FLAPPING TRIALS AT A PARTICULAR FLAPPING FREQUENCY. NOTE THAT FLAPPING FREQUENCIES RANGE FROM 5 - 15 HZ AND 3ω HARMONICS OF THE FLAPPING FREQUENCY RANGE FROM 15 - 30 HZ.

TABLE 3: STRAIN MAGNITUDE AT FLAPPING FREQUENCY AND THREE TIMES FLAPPING FREQUENCY FOR IN-AIR EXPERIMENTS AND CORRESPONDING STRAIN PREDICTIONS BY ONE-WAY AND TWO-WAY COUPLED FSI MODELS.

	$ \varepsilon(\omega) $ ($\mu\varepsilon$ p-p)	$ \varepsilon(3\omega) $ ($\mu\varepsilon$ p-p)
Theory, One-Way FSI	351	111
Theory, Two-Way FSI	350	69.0
Experiment (Air)	305	64.5

mation and aerodynamic forcing. This is the two-way coupled FSI model used for theoretic predictions in the previous section. While the two-way coupled model is more true-to-reality, one-way coupled models often provide good estimates of dynamics at reduced computational cost relative to two-way approaches. Thus, we investigate both of these cases and compare them to in-air experimental results. We now consider only a flapping frequency ω =10 Hz because this is where the 3ω response is most pronounced. We solve our EoM assuming both one-way and two-way coupled FSI and take the Fourier transform of the estimated physical strain. Results are shown in Table 3. We also show the predicted strain for one-way and two-way coupled models as a function of wingbeat fraction in Figure 9.

Clearly, the coupling between fluid and structure notably affects the wing's dynamics. While the primary strain response is nearly identical between one-way and two-way models, the two-way coupling model predicts a 3ω response that is 40% less than that predicted by the one-way model. Given the close agreement to the experiment, we believe the two-way coupled model is more accurate than the one-way coupled model. From this simulation, we conjecture that aerodynamic damping is a phenomena that cannot safely be neglected. It appears that aerodynamic damping affects higher-order harmonics of the wing response more so than its primary response.

CONCLUSION

The simple two-way coupled FSI model presented in this paper accurately predicts SDOF flapping dynamics and can be solved several orders of magnitude faster than conventional direct methods. This substantial reduction in computational time enables broad parametric studies considering variables such as wing geometry, flapping frequency and rotation amplitude. Consequently, this research informs studies in biological flight as well as the design of flapping-wing based technologies.

Through both experiment and simulation, we observe that

aerodynamic damping plays a significant role in attenuating higher-order harmonics of the wing's response. Two-way coupling between the fluid and structure is required to see this effect. The presence of aerodynamic damping likely has a significant impact on both artificial and biological flapping wing flight. Many insects flap at roughly 1/3 the fundamental frequency of their wings [23]. This flapping-to-natural frequency ratio is thought to improve aerodynamic performance [24, 25] and reduce the inertial costs of flight [22]. However, while compliance is generally viewed as favorable in the context of flapping wing flight, excessive flexibility may have adverse effects. It is plausible that fluid damping manages the wing's dynamic response and ensures that it does not deform so significantly that aerodynamic performance is compromised. Aerodynamic damping imparted by large flapping also safeguards higher-order vibration modes from being excited, which is especially important given that the linear damping ratio is very small for the stationary wing (Tab. 2).

Moving forward, we plan to generalize the two-way FSI model to accommodate more realistic MDOF flapping kinematics. This requires a more involved BET aerodynamic model that includes lift and rotational forces that arise from dynamic pitching. We will also compare this reduced-order approach to direct FSI methods to quantify increases in efficiency. Ultimately, this will elevate our knowledge of flapping wing flight.

Strain Magnitude vs. Wingbeat Fraction

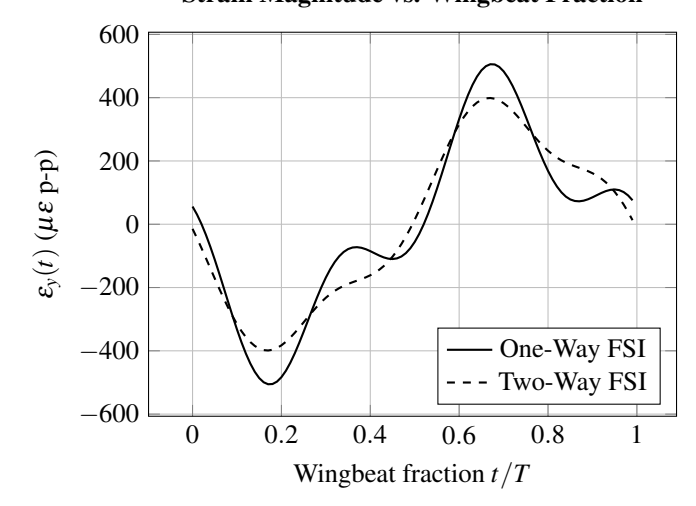


FIGURE 9: STRAIN PREDICTED BY ONE-WAY AND TWO-WAY COUPLED FSI MODELS AS A FUNCTION OF WINGBEAT FRACTION FOR A FLAPPING FREQUENCY OF 10 HZ.

ACKNOWLEDGMENT

This research was supported by Montana State University Norm Asbjornson College of Engineering. Travel to and dissemination of results at ASME IDETC/CIE 2019 was supported by the National Science Foundation under award No. CBET-1855383. Any opinions, findings, and conclusions or recommendations expressed in this material are those of the author(s) and do not necessarily reflect the views of the National Science Foundation.

REFERENCES

- [1] Shyy, W., Berg, M., and Ljungqvist, D., 1999. "Flapping and flexible wings for biological and micro air vehicles". *Progress in aerospace sciences*, *35*(5), pp. 455–505.
- [2] Mueller, T. J., 2001. Fixed and flapping wing aerodynamics for micro air vehicle applications. American Institute of Aeronautics and Astronautics.
- [3] Ellington, C. P., 1999. "The novel aerodynamics of insect flight: applications to micro-air vehicles". *Journal of Experimental Biology*, **202**(23), pp. 3439–3448.
- [4] Zhu, Q., and Peng, Z., 2009. "Mode coupling and flow energy harvesting by a flapping foil". *Physics of Fluids*, 21(3), p. 033601.
- [5] Zhu, Q., 2011. "Optimal frequency for flow energy harvesting of a flapping foil". *Journal of fluid mechanics*, **675**, pp. 495–517.
- [6] Xiao, Q., and Zhu, Q., 2014. "A review on flow energy harvesters based on flapping foils". *Journal of fluids and structures*, **46**, pp. 174–191.
- [7] Nakata, T., and Liu, H., 2012. "A fluid–structure interaction model of insect flight with flexible wings". *Journal of Computational Physics*, 231(4), pp. 1822–1847.
- [8] Shyy, W., Aono, H., Chimakurthi, S. K., Trizila, P., Kang, C.-K., Cesnik, C. E., and Liu, H., 2010. "in flapping wing aerodynamics and aeroelasticity". *Progress in Aerospace Sciences*, 46(7), pp. 284–327.
- [9] Ishihara, D., Horie, T., and Denda, M., 2009. "A two-dimensional computational study on the fluid–structure interaction cause of wing pitch changes in dipteran flapping flight". *Journal of Experimental Biology*, 212(1), pp. 1–10.
- [10] Gilmanov, A., Le, T. B., and Sotiropoulos, F., 2015. "A numerical approach for simulating fluid structure interaction of flexible thin shells undergoing arbitrarily large deformations in complex domains". *Journal of computational physics*, 300, pp. 814–843.
- [11] Tian, F.-B., Dai, H., Luo, H., Doyle, J. F., and Rousseau, B., 2014. "Fluid–structure interaction involving large deformations: 3d simulations and applications to biological systems". *Journal of computational physics*, *258*, pp. 451–460
- [12] Gresho, P. M., 1991. "Some current cfd issues relevant to the incompressible navier-stokes equations". *Computer*

- *Methods in Applied Mechanics and Engineering,* 87(2-3), pp. 201–252.
- [13] Jankauski, M., and Shen, I., 2014. "Dynamic modeling of an insect wing subject to three-dimensional rotation". *International Journal of Micro Air Vehicles*, **6**(4), pp. 231–251.
- [14] Sane, S. P., and Dickinson, M. H., 2002. "The aerodynamic effects of wing rotation and a revised quasi-steady model of flapping flight". *Journal of experimental biology*, **205**(8), pp. 1087–1096.
- [15] Whitney, J. P., and Wood, R. J., 2010. "Aeromechanics of passive rotation in flapping flight". *Journal of Fluid Mechanics*, **660**, pp. 197–220.
- [16] Jankauski, M., Daniel, T., and Shen, I., 2017. "Asymmetries in wing inertial and aerodynamic torques contribute to steering in flying insects". *Bioinspiration & biomimetics*, 12(4), p. 046001.
- [17] Berman, G. J., and Wang, Z. J., 2007. "Energy-minimizing kinematics in hovering insect flight". *Journal of Fluid Mechanics*, *582*, pp. 153–168.
- [18] Wang, Q., Goosen, J., and van Keulen, F., 2017. "An efficient fluid–structure interaction model for optimizing twistable flapping wings". *Journal of Fluids and Structures*, 73, pp. 82–99.
- [19] Stanford, B., Kurdi, M., Beran, P., and McClung, A., 2012. "Shape, structure, and kinematic parameterization of a power-optimal hovering wing". *Journal of Aircraft*, **49**(6), pp. 1687–1699.
- [20] Jankauski, M. A., 2018. "Low-order aeroelastic modeling of flapping, flexible wings". In ASME 2018 International Design Engineering Technical Conferences and Computers and Information in Engineering Conference, American Society of Mechanical Engineers, pp. V008T10A021– V008T10A021.
- [21] Elliott, S., Tehrani, M. G., and Langley, R., 2015. "Non-linear damping and quasi-linear modelling". *Philosophical Transactions of the Royal Society A: Mathematical, Physical and Engineering Sciences,* 373(2051), p. 20140402.
- [22] Jankauski, M., Guo, Z., and Shen, I., 2018. "The effect of structural deformation on flapping wing energetics". *Journal of Sound and Vibration*, **429**, pp. 176–192.
- [23] San Ha, N., Truong, Q. T., Goo, N. S., and Park, H. C., 2013. "Relationship between wingbeat frequency and resonant frequency of the wing in insects". *Bioinspiration & biomimetics*, 8(4), p. 046008.
- [24] Fitzgerald, T., 2013. "Nonlinear fluid-structure interactions in flapping wing systems". PhD thesis.
- [25] Dai, H., Luo, H., and Doyle, J. F., 2012. "Dynamic pitching of an elastic rectangular wing in hovering motion". *Journal of Fluid Mechanics*, **693**, pp. 473–499.